Influence of wheel polygonal wear on wheel-rail dynamic contact in a heavy-haul locomotive under traction conditions

Liang, Hongqin; Liu, Pengfei; Wang, Tianlong; Wang, Haoyu; Zhang, Kailong; Cao, Yunqiang; An, Dong

DOI
10.1177/0954409720931610

Publication date
2020

Document Version
Final published version

Published in
Proceedings of the Institution of Mechanical Engineers, Part F: Journal of Rail and Rapid Transit

Citation (APA)
Liang, H., Liu, P., Wang, T., Wang, H., Zhang, K., Cao, Y., & An, D. (2020). Influence of wheel polygonal wear on wheel-rail dynamic contact in a heavy-haul locomotive under traction conditions. *Proceedings of the Institution of Mechanical Engineers, Part F: Journal of Rail and Rapid Transit*, *235 (2021)*(4), 405-415. https://doi.org/10.1177/0954409720931610

Original Article

Institution of MECHANICAL ENGINEERS
Journal of RAIL AND RAPID TRANSIT

Proc IMechE Part F:
J Rail and Rapid Transit
2021, Vol. 235(4) 405–415

DOI: 10.1177/0954409720931610
journals.sagepub.com/home/pif
SAGE

Influence of wheel polygonal wear on wheel-rail dynamic contact in a heavy-haul locomotive under traction conditions

Hongqin Liang[1], Pengfei Liu[2], Tianlong Wang[2], Haoyu Wang[3], Kailong Zhang[2], Yunqiang Cao[2] and Dong An[1]

Abstract

For a heavy-haul locomotive within a wheel repairing period, wheel polygonal wear with different operating mileages is obtained by field testing. The test results show that the maximum radial runout of the wheel can increase to 0.87 mm and accompany with the typical damage of wheel tread shelling. Taking the wheel polygons as input excitation, the locomotive-track coupled dynamic model is established, which is verified by the comparisons of test and calculated wheelset vertical acceleration in time and frequency domains. The variable wheel-rail friction coefficient is introduced so as to consider the dry and wet rail conditions. The wheel-rail dynamic contact characteristics under the traction and dry-wet rail surface conditions are analysed simultaneously. It is found that the wheel polygon deteriorates the locomotive traction performance and induces the obvious wheel-rail slipping with large tangential stress, especially in wet rail condition. In dry condition, the wheel-rail could contact generally in the adhesion state. But the longitudinal creep forces fluctuate locally with some larger amplitudes closed to the adhesion force, which is mainly attributed to the excitation of serious wheel polygon. Comparing with the results of the newly repaired wheel, the maximum wheel-rail vertical force, longitudinal force, normal stress and tangential stress at the end of wheel repairing period can increase by 55 kN, 28 kN, 240 MPa and 470 MPa in sequence. The wheel-rail slipping and high-stress state in traction condition should be the dominant factors contributing to the wheel damage of tread shelling.

Keywords

Heavy-haul locomotive, wheel polygon, wheel-rail contact, traction

Date received: 27 October 2019; accepted: 26 April 2020

Introduction

With the development of the railway network, the passenger lines trend to separate from the freight line network and form its network. Heavy-haul railways are often used in freight transport, since it is an effective way to increase the carrying capacity. The features of heavy-haul trains include high carrying capacity, a large number of wagons, and long trains. Also, the tracks and wagons should be adjusted to adapt heavy-haul railways.[1]

One of the main problems commonly observed in heavy-haul railways after the operation is the uneven wear of wheels. As the wear grows, the shape of wheels gradually may develop into polygons, which may lead to higher impact between wheels and rails. In recent years, the wheel-rail fatigue damage and abnormal vibration of the HXD locomotive induced by wheel polygon were found frequently,[2,3] which significantly shorted the wheelset service life and even the wheel repairing period had to be reduced to 83,000 km. The relevant problems have been focused early in the 1990s. Pallgen[4] studied the initiation of the periodic and non-periodic wheel polygon and considered that the steel wheels and elastic rubber wheels respectively had the mainly 3rd and 2nd order

[1]Institute of Advanced Design & Manufacturing, Southwest Jiaotong University, Cheng Du, China
[2]State Key Laboratory of Mechanical Behavior and System Safety of Traffic Engineering Structures, Shijiazhuang Tiedao University, Shijiazhuang, China
[3]Faculty Of Civil Engineering and Geosciences, Delft University of Technology, Delft, the Netherlands

Corresponding author:
Hongqin Liang, Institute of Advanced Design & Manufacturing, Southwest Jiaotong University, Cheng Du, China.
Email: hongqinliang@swjtu.edu.cn

wheel polygon harmonics. As for the non-periodic wheel polygon, it consisted of many different orders. Brommundt[5] found that the wheel polygonal wear initiated and developed by the creep forces, and the low-order harmonics of wheel polygonal wear appeared more often at a higher train speed. some researchers[6,7] found that a large effect on high speed trains might be observed when the passing frequency of wheel polygon was between 50 and 500 Hz. Also, a single poygonalised wheel has a large influence on the other wheel of the same wheelset, even though the other one is perfectly circular. Recently, some researchers[8,9] found that the high-frequency normal and tangential wheel-rail forces would aggravate the track irregularity. In fact, both the rail corrugation and wheel polygon were the typical wheel-rail excitation sources in high frequency. Song et al.[10] and Liu et al.[11] believed that the wheel polygons also could cause large noise and serve wheel-rail coupling vibration. Han et al.[12] and Zhai et al.[13] analysed the effects of the polygonal wheel on the train-track-bridge system and found that the high order components of polygonal wear could threat the vehicle running safety and activate the abnormal vertical vibration of the bridge in middle or high-frequency ranges. Zou et al.[14] and Wu et al.[15] found that wheel polygon wear has been the main reason of the gearbox fatigue of and bogie vibration intensified in the high-speed train. Without exception, the increases in running speed and wheel polygonal amplitude could result in higher wheel-rail forces and accelerations. Wang et al.[16] investigated the influence of wheel polygon on the high-speed train passing through turnout, in which it was confirmed that the wheel-rail vertical force exceeded the safety limit as the wheel polygon amplitude reached 0.20 mm.

In general, the wheel polygon wear has become one of the main factors affecting the train dynamic behaviour, especially when the train running speed increases. With respect to the locomotive and freight wagon with low speed, the passenger vehicle has the higher requirements of ride qualities, which means the performance deterioration caused by wheel polygon could be fully reflected and felt in the high-speed train. The relevant research also indicates that the raising speed can significantly intensify the influence of wheel polygon. Therefore, most existing studies focus on the problem of wheel polygon in high speed train, while the wheel polygonal wear pattern and its dynamic effect on locomotive traction performance have not attracted enough attention. Particularly, the field tests of the wheel polygonal wear of heavy-haul locomotive have seldom been conducted. Therefore, this paper presents a study of the wheel-rail contact of heavy-haul locomotives (25 t), including field tests and numerical simulations. The polygonal wear of the wheels with various operating mileages are obtained, and then later used as the input excitation of the dynamic locomotive-track model. By considering the wet and dry states of the rail surface, the wheel-rail dynamic contact characteristics under the driving condition are studied. Finally, the influence of wheel polygon evolution is discussed.

Field measurement of the wheel polygon

For a single locomotive, the tracking measurement of wheel polygon has been carried out as given in Liu et al.,[17] which indicates that the polygons of different wheels present different amplitudes. From the aspect of statistics, to understand the general evolution laws of wheel polygon wear of HXD locomotives running in the same line, the field test for wheel polygons of different locomotives with different mileage have been measured, as shown in Figure 1. Meanwhile, the phenomenon of tread shelling has been observed frequently. All of the test wheels had a diameter of 1250 mm and the test position locates in the wheel

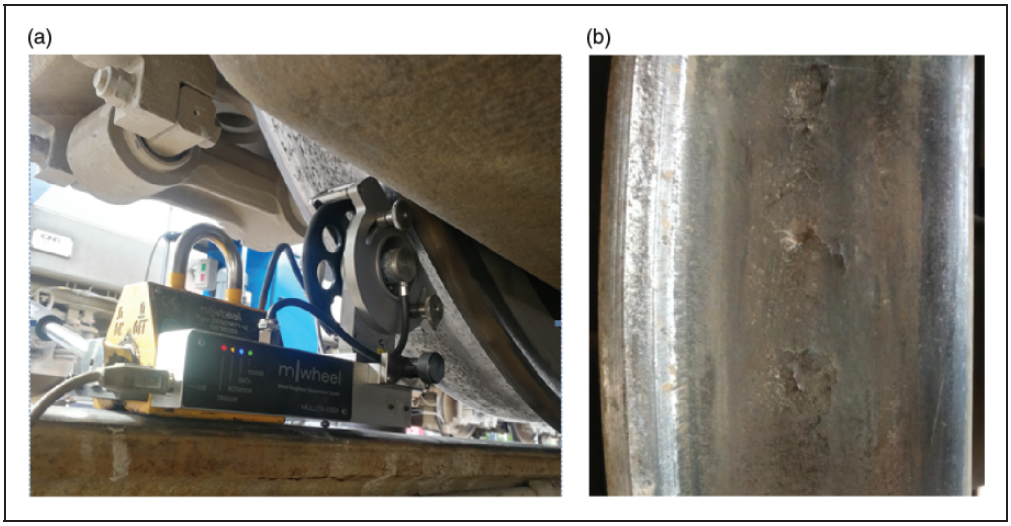

Figure 1. Field test of wheel polygon: (a) test scene; (b) tread shelling.

nominal rolling circle. The measuring device used is the wheel roughness meter with the accuracy of 0.1 μm and the sampling interval of 1 mm.

A number of locomotives with various operating mileages have been measured, which ranges from 0 km to 1.7×10^4 km, including 0 km, 3.4×10^4 km, 4.3×10^4 km, 7.7×10^4 km, 10×10^4 km, 1.2×10^4 km, and 1.7×10^4 km. Six wheel samples with different running distances are randomly chosen to reflect the typical wheel polygons, as shown in Figure 2, where the 0 km represents the wheel just after repairing and the negative value denotes the local depression. The wheel radial runout is defined as the difference between the maximum and minimum values of polygon amplitude, as shown in Figure 2(b). Generally, the radial runout increases significantly as the operating mileage grows.

In order to understand the general evolution status of wheel polygon, the test and analysis are carried out from the aspect of statistic. A total of 84 wheel polygons are given and their radial deviation distributions are compared in Figure 3. It can be found, the maximum radial runout values of the locomotive in case of 1.7×10^4 km can reach 0.603 mm, 0.706 mm, and even 0.87 mm. There are still no clear rules for locomotive wheel polygon in China. However, it is explicitly stipulated that, for the ordinary railway locomotive, the depths of wheel flat and tread shelling cannot exceed the limits of 0.7 mm and 1 mm respectively according to China Railway Corporation.[18] That means the maximum radial runout has exceeded the corresponding limit of wheel flat and is closed to the limit value of tread shelling. The radial runout values of the locomotive with 0 km are all below 0.05 mm, which means the condition of the wheel tread is significantly improved by the wheel repair. Based on the results in Figure 2, the maximum, mean and minimum values of 12 wheel polygon samples in different service distances are calculated, as shown in Figure 4. Both the radial deviation magnitude and its fluctuation range presents clear amplification with the running distance increasing. For example, in the case of 0 km and 17×10^4 km, the differences between maximum and minimum can change from 0.04 mm to 0.65 mm. The wheel circumferential wear has a relatively rapid developing rate.

In the following, the three wheels which have the serious polygon wear marked in Figure 3 are selected for further analysis, as shown in the polar coordinates in Figure 5(a). Through the discrete Fourier transform (DFT), the order of polygon change and the roughness level in the frequency domain can be obtained.[19] The wheel polygon order spectrum (1st to 19th) are shown in Figure 5(b). As shown in Figure 3, the wheel polygon with the 0.603 mm radial runout has an obvious quadrilateral feature, and the harmonic components mainly distribute in the 1st, 2nd, 3rd and 4th orders. Differently, the wheel polygon with the radial deviation of 0.706 mm presents as an octagon. Its corresponding harmonic

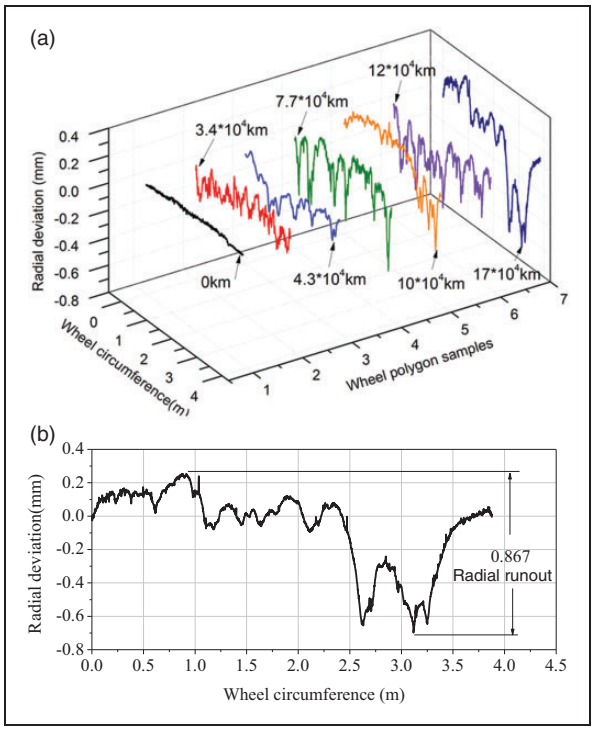

Figure 2. Wheel polygons of different mileage: (a) samples (b) definition of radial runout.

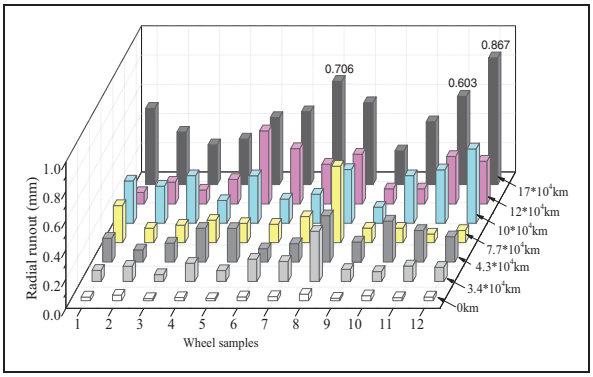

Figure 3. Radial deviation distribution for different operating mileages.

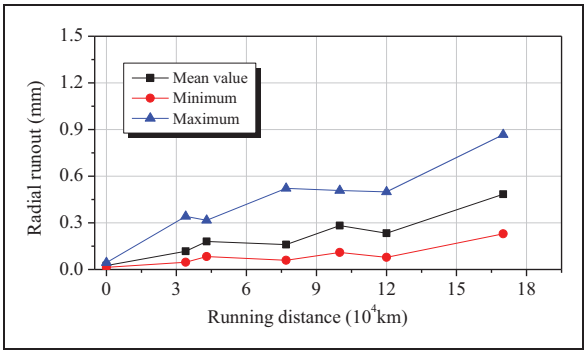

Figure 4. Statistical results of wheel radial runout.

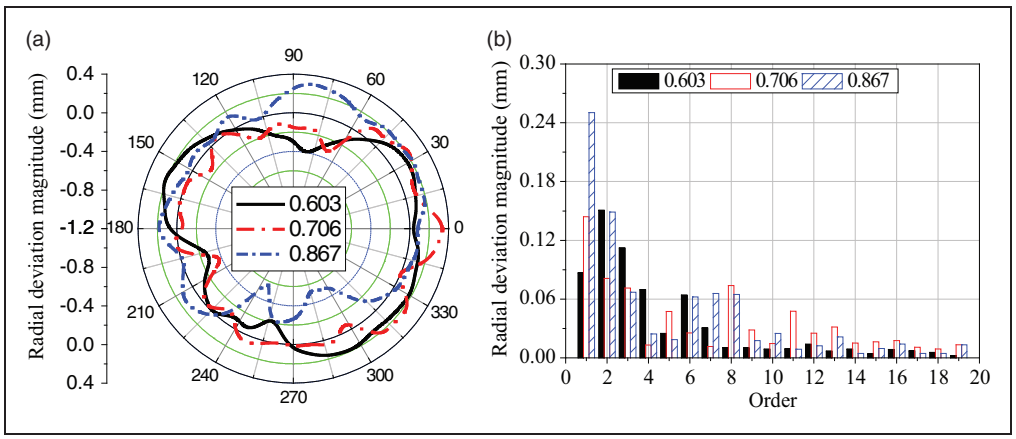

Figure 5. Serious wheel polygon wear: (a) wheel polygon; (b) order spectrum.

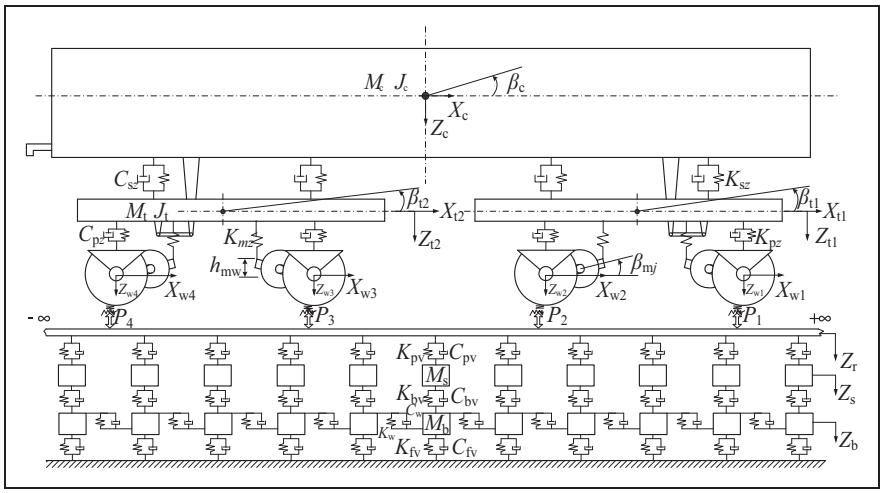

Figure 6. Side view of the locomotive-track model.

components are the 1st, 2nd, 3rd and 8th orders. The wheel polygon with the radial runout of 0.87 mm has a long-wave defect in the circumferential direction, the amplitude of the wave can reach 0.5 mm. The harmonic component of the 1st order takes the dominant position, which is much larger than the others.

Generally, the harmonic components of the measured wheel polygon are mainly in the 1st–3rd order and followed by the 6th-8th order. The harmonic components of the 1st-8th order correspond to the wavelengths ranging from 475 mm to 3890 mm, which can excite the vertical vibration of the locomotive from 4 to 70 Hz, if the locomotive normal running speed reaches 60 to 120 km/h. Actually limited by the line conditions, the running speed in the test line is below 80 km/h.

Numerical model

To study the wheel-rail dynamic interaction of polygonal wheels, a dynamic locomotive-track model has been developed based on the vehicle-track coupled dynamic theory.[20] The dynamic model considers both the vertical and longitudinal motions of the locomotive. The locomotive is modelled as the multi rigid bodies. The car body, bogies, and wheelsets are connected by primary and secondary suspensions, and traction rods. The side view and top view of the model are shown in Figures 6 and 7, respectively.

The locomotive model has 25 DOFs (Degree of Freedom), which contains the vertical, longitudinal, and pitch movement of the carbody; vertical and longitudinal movement of wheelsets, as shown in Table 1. Since the motor suspension is considered as axle suspension, only the rotation around the axle is considered. The track model considers the vertical movements of the rail, sleepers and the ballast. The parameters of the vehicle and track are shown in Table 2.

For the motion equations of the car body and bogie frame, they can be derived conveniently according to Zhai.[20] The wheelset and motor are connected by the axle suspension bearing which limits their relative motions in the longitudinal and vertical direction. So there are the dependent motions in the wheelset-motor subsystem. For that reason, the

longitudinal, vertical, pitching motion of wheelset are given in equations (1) to (3). Equation (4) represent the pitching equation of traction motor. The driving condition is considered during the simulation. The motor provides traction by applying tractive torque (M_q) to wheelsets. At the same time, an opposite force with the equal magnitude is applied to the coupler part of the carbody to simulate the running resistance, so that the locomotive can be kept in an equilibrium state in the longitudinal direction. which can be used to study the dynamic behaviour on the wheel-rail surface.

$$M_w\ddot{X}_{wi} - M_m h_{mw}\ddot{\beta}_{mi} = F_{wxi} + F_{xfi} + F_{mxi} \tag{1}$$

$$\begin{aligned}(M_w + M_m)\ddot{Z}_{wi} - (-1)^i M_m l_1\ddot{\beta}_{mi} \\ = -P_i + F_{mzi} + F_{zfi} + (M_w + M_m)g\end{aligned} \tag{2}$$

$$J_w\ddot{\beta}_{wi} = rF_{wxi} - M_q \tag{3}$$

$$\begin{aligned}(J_m + M_m l_1^2)\ddot{\beta}_{mi} - (-1)^i M_m l_1\ddot{Z}_{wi} - M_m h_{mw}\ddot{X}_{wi} \\ = (-1)^{i-1}F_{mzi}(l_1 + l_2) + (-1)^i F_{mxi}h_{dw} + M_q\end{aligned} \tag{4}$$

where F_{wxi} and F_{zfi} represent the wheel-rail longitudinal force and primary vertical force in order. The longitudinal and vertical suspension forces of traction motor can be expressed as

$$\begin{aligned}F_{mxi} = K_{mx}[X_{tn} - X_{wi} + h_{mw}\beta_{mi} + h_{tm}\beta_{tn}] \\ + C_{mx}[\dot{X}_{tn} - \dot{X}_{wi} + h_{mw}\dot{\beta}_{mi} + h_{tm}\dot{\beta}_{tn}]\end{aligned} \tag{5}$$

$$\begin{aligned}F_{mzi} = K_{mz}[Z_{tn} - Z_{wi} + (-1)^i(l_t - l_1 - l_2)\beta_{tn} \\ + (-1)^i(l_1 + l_2)\beta_{mi}] \\ + C_{mz}[\dot{Z}_{tn} - \dot{Z}_{wi} + (-1)^i(l_t - l_1 - l_2)\dot{\beta}_{tn} \\ + (-1)^i(l_1 + l_2)\dot{\beta}_{mi}]\end{aligned} \tag{6}$$

The longitudinal creep force is calculated by Fastsim, using the simplified Kalker theory.[21] The calculation of the normal contact force is based on the classical Hertzian nonlinear contact theory, wherein the input is a geometry parameter of the wheel tread at the nominal rolling circle. The wheel polygon is considered in the calculation of wheel-rail vertical force, as equation (7). It is input into the

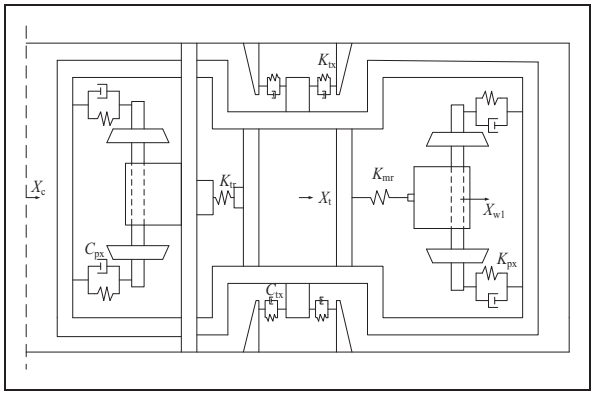

Figure 7. Top view of the bogie model.

Table 1. DOFs of the locomotive.

	Longitudinal	Vertical	Pitch
Wheelsets (i = 1 ~ 4)	X_{wi}	Z_{wi}	β_{wi}
Bogie	X_{tn}	Z_{tn}	β_{tn}
Motor	–	–	β_{mi}
Carbody	X_c	Z_c	β_c

Table 2. Parameters of the locomotive-track model.

Meaning	Notation	Unit	Value
Mass of carbody	M_c	kg	62600
Mass of bogie	M_t	kg	5114
Mass of wheelset	M_w	kg	3131
Mass of motor	M_m	kg	3662
Inertia of pitch movement of carbody	J_c	Kg×m^2	1221057.3
Inertia of pitch movement of Bogie	J_t	Kg×m^2	16778
Inertia of pitch movement of wheelset	J_w	Kg×m^2	433
Inertia of pitch movement of motor	J_m	Kg×m^2	801
Longitudinal stiffness and damping of primary suspension	K_{px}, C_{px}	MN/m, N×s/m	50.0 × 2, 2500 × 2
Vertical stiffness and damping of primary suspension	K_{pz}, C_{pz}	MN/m, N×s/m	1.57, 25000
Longitudinal stiffness and damping of secondary suspension	K_{tx}, C_{tx}	MN/m, N×s/m	0.16 × 2, 10000 × 2
Vertical stiffness and damping of secondary suspension	K_{tz}, C_{tz}	MN/m, N×s/m	1.07, 45000
Longitudinal distance from motor mass center to suspending point and wheelset	l_1, l_2	m, m	0.47, 0.701
Vertical distance between mass centers of motor and wheelset	h_{mw}	m	0
Vertical distance between mass centers of motor and bogie frame	h_{tm}	m	0.216
Longitudinal stiffness and damping of motor suspending rod	K_{mx}, C_{mx}	MN/m, N×s/m	0.05, 1000
Vertical stiffness and damping of motor suspending rod	K_{mz}, C_{mz}	MN/m, N×s/m	5.0, 1000

dynamic model as the track irregularity and affects the locomotive-track coupling vibration by changing the wheel-rail vertical forces.

$$P_i(t) = \left[\frac{1}{G}\left(Z_{wi}(t) - Z_r(X_{wi}, t) - Z_{pi}(t)\right)\right]^{3/2} \quad (7)$$

where G is the contact constant, $Z_r(X_{wi}, t)$ represents the rail vertical displacement below the ith wheel at time t. $Z_{pi}(t)$ denotes the wheel polygon of the ith wheel.

For the calculation of wheel-rail contact tangential force, according to the Kalker simplified theory,[21] it is assumed that the tangential stress in rolling direction can be expressed as equation (8). And the pressure stress can be calculated by equation (9). By the elliptic integration of tangential stress, the final wheel-rail longitudinal force is given in equation (10).

$$\begin{cases} p_1(x,y) = \left(\frac{\xi_1}{L_1} - \frac{\xi_3 y}{L_3}\right)\left(x - a\sqrt{1-\left(\frac{y}{b}\right)^2}\right) & p_1(x,y) < up_3 \\ p_1(x,y) = \mu p_3 & p_1(x,y) \geq up_3 \end{cases} \quad (8)$$

$$p_3 = \frac{2P_i}{\pi ab}\left(1 - \frac{x^2}{a^2} - \frac{y^2}{b^2}\right) \quad (9)$$

$$F_{wxi} = \int\int_d p_1 \mathrm{d}x\mathrm{d}y = -\frac{8a^2 b}{3L_1}\xi_1 \quad (10)$$

where ξ_1 and ξ_3 are the longitudinal and spin creepages respectively. L_1 and L_3 denote the flexibility coefficients in longitudinal and spin direction. a and b are the lengths of contact patch semi axis in longitudinal and lateral directions. x and y are the coordinate values of contact patch grindings. In the locomotive-track coupled dynamic model, the lateral and spin creepages have not been taken into account, so that the tangential stress is proportional to the longitudinal creepage.

The computer program is developed based on Fortran, which spends the computational time about 3.2 s for the actual running time of 1 s. To validate the dynamic model, the vertical vibration of wheelset excited by wheel polygon is tested.[22] Under the same wheel polygon wear, the wheelset vibration is simulated. Both the test and simulated wheelset vertical accelerations in time and frequency domain are compared in Figure 8, where the data is given for wheel rotating a circle. For the time responses, the test and simulation results have a similar amplitudes within ±1.5 g. For the frequency responses, the test and calculated results present similar changing rules and cover the same dominant frequency. Indeed, the track irregularity and some minor defects distribute in the actual spatial curved surface of wheel and rail profiles, which leads to the difference between test and calculated results. However, the general vibration excited by the wheel polygon has been reflected adequately in the numerical model.

Influence of wheel polygon on traction in wet and dry rail conditions

Using the numerical model presented in Section 'Numerical model', the wheel-rail contact under the dry and wet conditions is studied. To reflect the wheel-rail dynamic interaction in the case of serious wheel polygon wear, the largest radial runout (Figure 2(b)) collected in the onsite measurement is regarded as the wheel-rail excitation. The locomotive running speed is set as 60 km/h, and the corresponding traction force for the locomotive running stably is approximately 290 kN. The dynamic friction coefficient is calculated as equation (11),[23] where the wheel-rail creep speed in the dynamic model can be expressed the variables and values under various humidity conditions are shown in Table 3.

$$\mu = \mu_0\left[(1-A)e^{-B\omega} + A\right] \quad (11)$$

$$\omega = \left|r\dot{\beta}_{wi} - \dot{X}_{wi}\right| \quad (12)$$

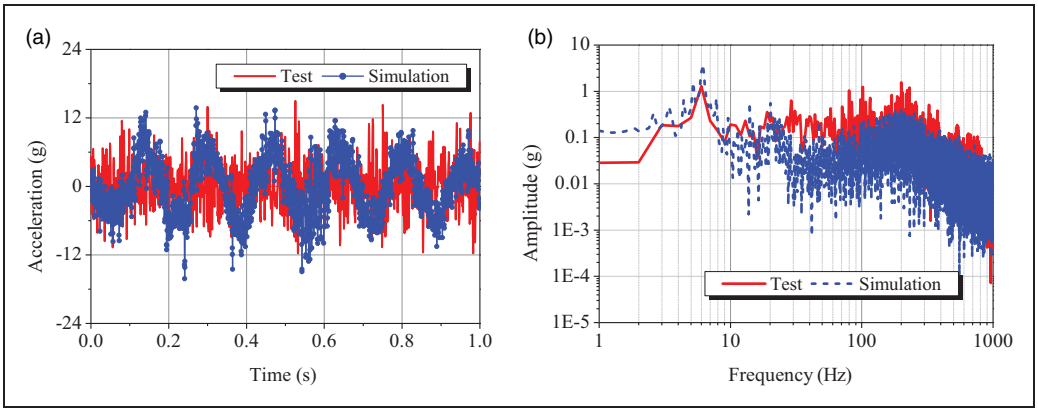

Figure 8. Comparisons of wheelset vertical acceleration in (a) time domain and (b) frequency domain.

Table 3. Variables and values.

Notation	Meaning	Rail surface state	
		Dry	Wet
μ	Calculated coefficient of friction		
μ_0	Maximum friction coefficient at zero slip velocity	0.55	0.30
A	Friction coefficient ratio	0.40	0.40
B	Coefficient of exponential friction decrease (s/m)	0.60	0.20
w	Total creep speed between wheel and rail		

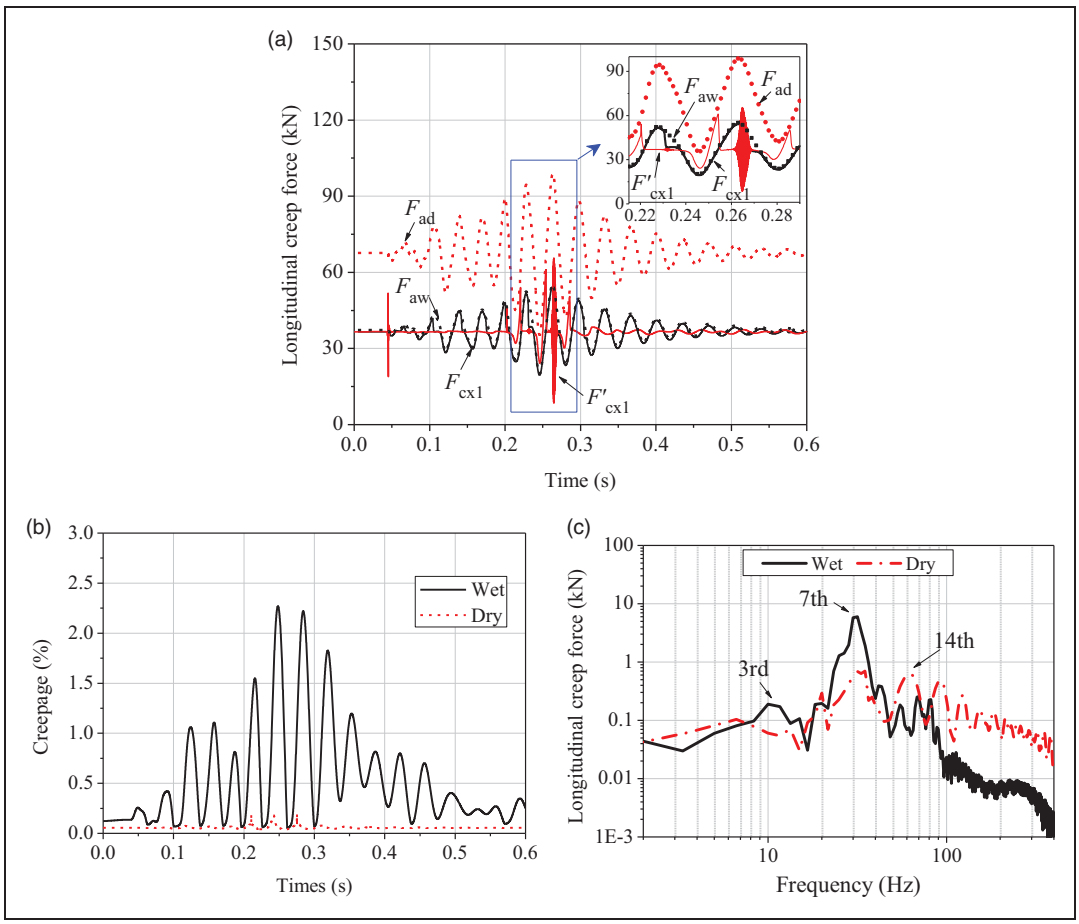

Figure 9. Wheel-rail adhesive state and forces in the dry and wet rail condition: (a) wheel-rail longitudinal forces, (b) creepage, (c) spectrum properties of creep forces.

The effect of the rail surface on the wheel-rail dynamic behaviour is analysed by using the various parameters in equation (11) as input. The calculated creep forces under dry and wet condition are shown in Figure 9, where F_{aw} and F_{ad} represent the adhesion limit in dry and wet conditions. F_{cx1} and F'_{cx1} denote the actual wheel-rail longitudinal creep forces in the two corresponding rail states. As shown in Figure 9 (a), the longitudinal creep force fluctuates in a wider range under the wet condition, but the amplitudes are larger for dry rail surface. It can be found clearly in both Figure 9(a) and (b) that, the creep forces for wet rail could reach to the adhesion limit force in most time, accompanying with the larger wheel-rail creepage. That means the wheel-rail stick-slip states switch frequently, and the wheel-rail sliding phenomenon occurs obviously. The small wheel-rail friction coefficient determines the above phenomenon directly. Comparatively in dry condition, the adhesion limit increases due to the larger friction coefficient, which can ensure the wheel-rail contact works generally in the adhesion state. But inevitably, the slight increase of creepage still induces some local larger longitudinal forces under the excitation of wheel polygon, even though the creepage is much lower than the maximum values in wet condition. No matter how the rail

surface states change, the wheel polygonal wear can deteriorate the locomotive adhesive performance significantly, especially when the rail gets wet in rain or snow weather. From the spectrum of the frequency domain, the spectrogram in Figure 9(c) shows that the main frequency appears around 30 Hz under both the dry and wet conditions. The frequency of 30 Hz corresponds to the 7th order wheel polygon, and the two side frequencies 10 Hz and 60 Hz to the 3rd and 14th order.

The dry and wet condition of the rail surface also has an effect on the wheel-rail tangential stress. The maximum of tangential stress in wet and dry rail conditions are compared in Figure 10. In the wet condition, the stress with the maximum of 635 MPa is higher in most time with respect to that in dry condition, which is mainly determined by the corresponding large creepage. However, the stress would be limited by the relatively small adhesive force. In dry condition, once the dynamic wheel-rail tangential force is closed to the relatively high adhesion limit, the large creep force and tangential stress may occur. That is the main reason that the stress in the dry condition is larger and cover a wider range from 67 MPa to 907 MPa. Generally, the maximum stress in the dry condition is approximately 1.5 times comparing to that under the wet condition. The main frequency in the spectrogram also appears at around 30 Hz and a side frequency appears at 60 Hz, which corresponds to the 7th and 14th order of the wheel polygon respectively.

The reduction of maximum creep force in the wet condition is determined by the small friction coefficient, when the wheel-rail pressure is unchanged. As the rail surface is kept in the dry state, the friction coefficient is larger, which results in the large fluctuation of wheel-rail tangential stress under the wheel polygon excitation. It can also be found that the harmonics of different orders have different effects on the wheel-rail dynamics behaviour, wherein the 7th order has the most significant impact.

Influence of wheel polygon evolution on traction performance

In order to study the influence of wheel polygon evolution on the locomotive traction performance, the analysis is carried out from the aspect of the system vibration and wheel-rail contact. To explain the effect clearly, some indices, such as vibration acceleration, wheel-rail longitudinal force, vertical force, normal and tangential stress have been given. Three typical radial deviations with 0 km, 7.7×10^4 km and 17×10^4 km are applied as the input excitation of the numerical model, which are represented by 0, 77 k and 170 k.

Firstly, the wheelset vertical acceleration is compared in the three cases, as shown in Figure 11. The acceleration induced by the wheel polygon with (0 km) is very small and below 0.2 m/s^2. While the operating mileage extends to 77,000 km and 170,000 km, the vertical accelerations can reach $\pm$ 2.06 m/s^2 and $\pm$3 m/s^2. The spectrogram shows that the same peak at around 30 Hz appears in all cases, corresponding to the 7th wheel polygon harmonic.

The longitudinal accelerations of wheelsets in three cases are compared in Figure 12. The wheel polygon of 77,000 km has little effect on the longitudinal acceleration which is below 0.6 m/s^2. As the running distance increase to 170,000 km, the wheelset acceleration covers the range from –1.26 m/s^2 to 1.18 m/s^2. In the spectrogram, the dominant frequency is 36 Hz, which corresponds to the 8th harmonics. In addition, multiple side frequencies of 10 Hz, 21 Hz, 62 Hz, and 93 Hz can be also found, corresponding to the 3rd, 5th, 16th, and 19th wheel polygon harmonics.

From the aspect of wheel-rail dynamic interaction, the wheel-rail vertical and longitudinal forces excited by the different wheel polygons are compared in Figure 13, where the corresponding maximum values are also given. The evolution of wheel polygon results in more serious wheel-rail coupling vibration. For the service mileage in 0 km, 77k km and 170k km, the wheel-rail vertical force increases from 125 kN to

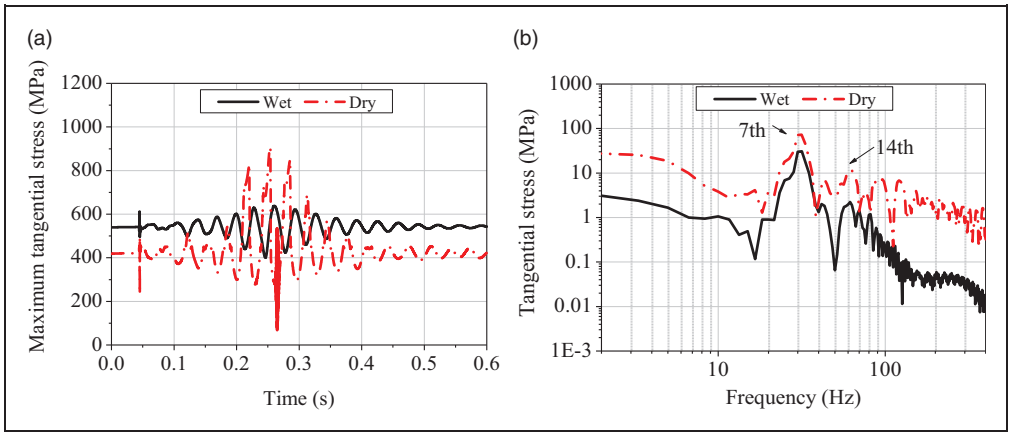

Figure 10. Wheel-rail tangential stress in dry and wet rail condition: (a) time response, (b) spectrum characteristic.

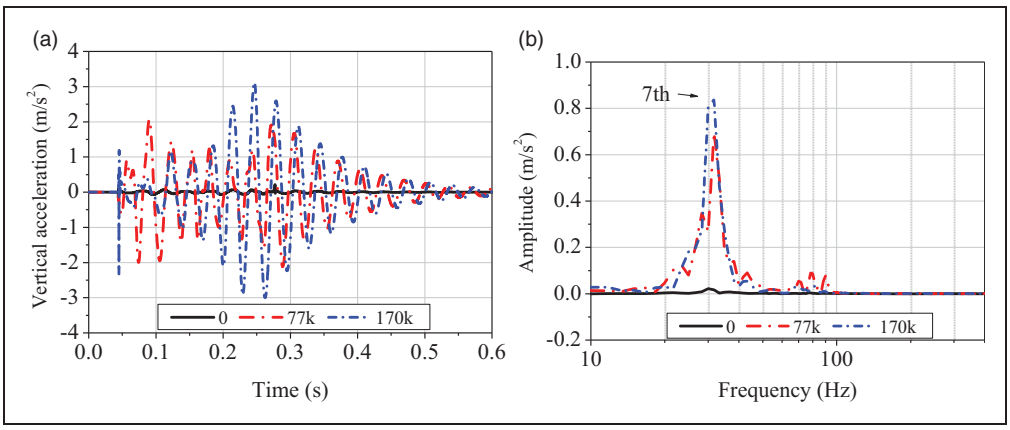

Figure 11. Vertical acceleration of wheelsets: (a) time response, (b) spectrum characteristic.

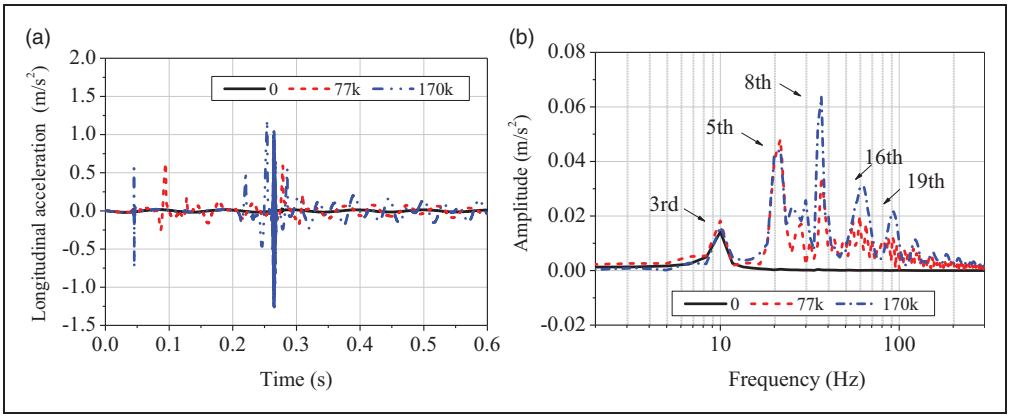

Figure 12. Longitudinal acceleration of wheelsets: (a) time response, (b) spectrum characteristic.

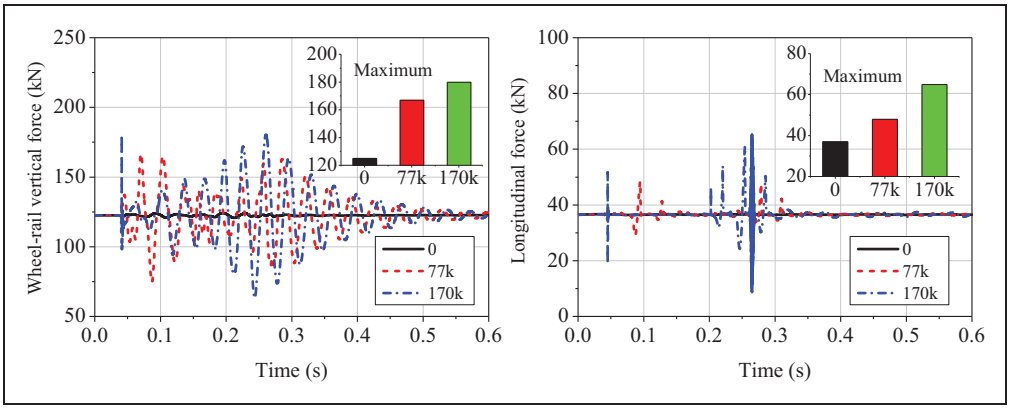

Figure 13. Wheel-rail dynamic force comparison for different polygon samples: (a) vertical forces; (b) longitudinal creep forces.

167 kN and 180 kN. Correspondingly, the peak value of longitudinal creep force changes from 37 kN to 48 kN and 65 kN. Affected by the evolution of wheel polygon in a wheel repairing period, the maximum increments of 55 kN and 28 kN are observed in the wheel-rail vertical and longitudinal forces, which means the traction stability of locomotive has been deteriorated.

As for the wheel-rail normal and tangential contact stress, the time histories of their peak value in the contact patch are observed, as shown in Figure 14. And then, the maximums for different wheel polygons are compared. For service mileage of 0 km, 77k km and 170k km, the wheel-rail normal stress can reach 1413 MPa, 1597 MPa and 1653 MPa respectively, while the corresponding tangential stress increases

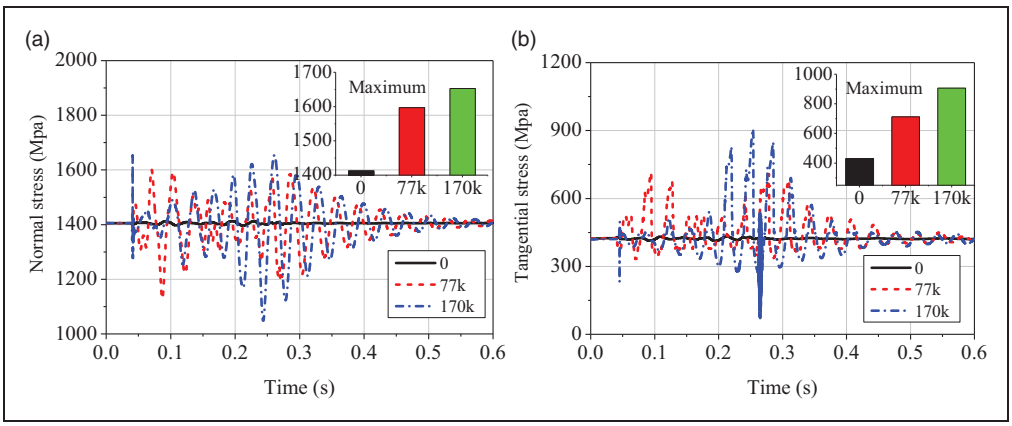

Figure 14. Wheel-rail contact stress comparison for different polygon samples: (a) normal stress; (b) tangential stress.

from 431 MPa to 713 MPa and 907 MPa. In a wheel repairing period, both the contact stresses in the normal and tangential direction increase by about 240 MPa and 470 MPa. To a great extent, the wheel tread shelling shown in Figure 14(b) can be contributed to the significant high stress induced by the wheel polygon wear. From another perspective, the intense wheel-rail dynamic interaction and high stress conversely could accelerate the wheel polygon evolution.

In summary, both the vertical and longitudinal vibrations of wheel-rail contact have been deteriorated significantly as the wheel polygon increases. The problems of wheel-rail slipping, coupling vibration and high-stress state in traction condition become difficult to avoid, which could be the dominant factors contributing to the wheel damage of tread shelling. From the view of wheel polygon influence, with the growth of operating mileage, the harmonics of 7th and 8th orders have the largest effect. Moreover, the 170,000 km operating mileage wheelsets cause considerable longitudinal acceleration, which is influenced by many harmonics, including the 8th, 5th, 16th, 19th, and 3rd.

Conclusions

For the heavy-haul locomotives in China, the field test and dynamic influence analysis of wheel polygon are carried out. Some conclusions can be drawn as below.

1. The radial derivation increases significantly as the wheelset operating mileage grows. Within a wheel repairing period, the maximum test radial runout can reach 0.87 mm, which has exceeded the corresponding limit of wheel flat (0.7 mm) and is closed to the limit value of tread shelling (1 mm). The harmonic components of the measured wheel polygon mainly concentrate on the 1st-3rd order and followed by the 6th-8th order.
2. The wheel polygon will deteriorate the locomotive traction performance and induce the problem of wheel-rail slipping. If the traction is applied in the wet rail condition, the traction force is closed to the adhesion limit, and the wheel-rail slipping phenomenon occurs obviously. In dry condition, the adhesion limit increases, and the wheel-rail contact works generally in the adhesion state. But some local larger longitudinal forces still occur under the excitation of wheel polygon.
3. With respect to the results of the newly repaired wheel, the peak values of wheel-rail vertical force, longitudinal force, normal stress and tangential stress in the repairing period end increase by 55 kN, 28 kN, 240 MPa and 470 MPa in sequence. The problems of wheel-rail slipping and high-stress state in traction condition become difficult to avoid, which could be the dominant factors contributing to the wheel damage of tread shelling. From the view of wheel polygon influence, the 7th and 8th harmonics have the largest effect.

Data availability statement

The data used to support the findings of this study are available from the corresponding author upon request.

Declaration of Conflicting Interests

The author(s) declared no potential conflicts of interest with respect to the research, authorship, and/or publication of this article.

Funding

The author(s) disclosed receipt of the following financial support for the research, authorship, and/or publication of this article: The present work is supported by the National Natural Science Foundation of China (Nos. 11790282, 51605315), the Sichuan Science and Technology Program of China (No. 2019YFH0053) and the Natural Science Foundation of Hebei Province (Grant No. E2018210052).

ORCID iD

Hongqin Liang https://orcid.org/0000-0002-5252-7862

References

1. Lyu J, Guo QY and Fu YM. Research on the process of dynamic modeling and simulation for heavy haul train. *Electric Drive for Locomotives* 2015; 06: 26–29.
2. Liu W, Yan N, Pu QW, et al. Development trend of wheel set polygon on Type HXD1 locomotive. *Electric Locomotives & Mass Transit Vehicles* 2017; 40: 55–59.
3. Wang J. Discussion on Fix-method of out of roundness wheel HXD3C. *Railway Locomotive & Car* 2018; 38: 101–105.
4. Pallgen G. Unrunde rader an eisenbahnfahraeugen. *Der Eisenbahningenieur* 1998; 49: 56–60.
5. Brommundt E. A simple mechanism for the polygonalization of railway wheels by wear. *Mech Res Commun* 1997; 24: 435–442.
6. Kaiser I and Popp K. *Modeling and simulation of the mid-frequency behaviour of an elastic bogie*. Berlin: Springer, 2003.
7. Popp K, Kaiser I and Kruse H. System dynamics of railway vehicles and track. *Arch Appl Mech* 2003; 72: 949–961.
8. Johansson A and Nielsen J. Rail corrugation growth – influence of powered wheelsets with wheel tread irregularities. *Wear* 2007; 262: 1296–1307.
9. Baeza L, Vila P, Roda A, et al. Prediction of corrugation in rails using a non-stationary wheel-rail contact model. *Wear* 2008; 265: 1156–1162.
10. Song ZK, Yue RF, Hu XY, et al. Influence of wheel polygon on vehicle vibration and wheel/rail force. *J Beijing Jiaotong Univ* 2017; 41: 88–93.
11. Liu ZY, Gao CY, Yin XM, et al. of Abnormal vibration and noise on Beijing Metro Line 14 and improvement measures. *Urban Mass Transit* 2018; 21: 74–77.
12. Han ZL, Chen ZW and Zhai WM. Effect of wheel polygonal wear on dynamic responses of high speed train-track-bridge system. In: *Proceedings of the 25th International Symposium on Dynamics of Vehicles on Roads and Tracks*, pp.823–828. New York: CRC Press, 2017.
13. Zhai WM, Han ZL, Chen ZW, et al. Train-track-bridge dynamic interaction: a state-of-the-art review. *Vehicle Syst Dyn* 2019; 57: 984–1027.
14. Zou HY, Zhang WH and Wang ZW. Influence of wheel polygonization on dynamic response of gearbox housing of high-speed train. *Electric Drive Locomot* 2017; 6: 52–56.
15. Wu Y, Han J, Liu J, et al. Effect of high-speed train polygonal wheels on wheel/rail contact force and bogie vibration. *Jme* 2018; 54: 37–46.
16. Wang P, Zhang RH, Chen JY, et al. Influence of polygonal wheels in high-speed trains on dynamic performance of turnout. *Jme* 2018; 54: 47–56.
17. Liu P, Wang T, Lü K, et al. Wheel polygon evolution and dynamic influence on heavy haul locomotive. *Chin Sci Bull* 2019; 64: 2583–2589.
18. China Railway Corporation. *Regulations of railway technical operation*. Beijing: China Railway Publishing House, 2014.
19. Johansson A. Out-of-round railway wheels – assessment of wheel tread irregularities in train traffic. *J Sound Vibration* 2006; 293: 795–806.
20. Zhai WM. *Vehicle-track coupled dynamics*. 4th ed. Beijing: Science Press, 2015.
21. Kalker JJ. A fast algorithm for the simplified theory of rolling contact. *Vehicle Syst Dyn* 1982; 11: 1– 13.
22. Wang TL, Liu PF, Zhang KL, et al. Research of wheel-rail coupled vibration excited by wheel polygon for heavy-haul locomotive. *IOP Conf Ser: Earth Environ Sci* 2018; 189: 062026.
23. Polach O. Creep forces in simulations of traction vehicles running on adhesion limit. *Wear* 2005; 258: 992–1000.